



1 Characterisation of the transfer of cluster ions through an 2 Atmospheric Pressure interface Time-of-Flight mass spectrometer 3 with hexapole ion guides

4 Markus Leiminger^{1,2}, Stefan Feil², Paul Mutschlechner², Arttu Ylissirniö³, Daniel Gansch², Lukas Fischer¹,
5 Alfons Jordan², Siegfried Schobesberger³, Armin Hansel^{1,2} and Gerhard Steiner^{1,4}

6
7 ¹University of Innsbruck, Institute of Ion Physics and Applied Physics, 6020 Innsbruck, Austria

8 ²Ionicon Analytik GmbH, 6020 Innsbruck, Austria

9 ³University of Eastern Finland, Department of Applied Physics, 70211 Kuopio, Finland

10 ⁴Grimm Aerosol Technik Ainring GmbH & Co. KG, 83404 Ainring, Germany

11

12 *Address correspondence to:* G. Steiner (gerhard.steiner@uibk.ac.at) and A. Hansel (armin.hansel@uibk.ac.at)

13

14 **Abstract.** Here we present an alternative approach of an Atmospheric-Pressure interface (APi) Time-Of-Flight mass
15 spectrometer for the study of atmospheric ions and cluster ions, the so-called ioniAPi-TOF. The novelty is the use of two
16 hexapoles as ion guides within the APi. As we will show, hexapoles can accept and transmit a broad mass range enabling the
17 study of small precursor ions and heavy cluster ions at the same time. Weakly bound cluster ions can easily de-cluster during
18 ion transfer depending on the voltages applied to the ion transfer optics. With the example system of $\text{H}_3\text{O}^+(\text{H}_2\text{O})_{n=0-3}$, we
19 estimate that cluster ions with higher binding energies than 17 kcal/mol can be transferred through the APi without significant
20 fragmentation, which is considerably lower than about 25 kcal/mol estimated from the literature for APi-TOFs with quadrupole
21 ion guides. In contrast to the low fragmenting ion transfer, the hexapoles can be set to a high fragmenting declustering mode
22 for collision-induced dissociation (CID) experiments as well. The ion transmission efficiency over a broad mass range was
23 determined to be in the order of 1%, which is comparable to existing instrumentation. From measurements under well-
24 controlled conditions during the CLOUD experiment, we demonstrate the instrument's performance and present results from
25 an inter-comparison with a quadrupole based APi-TOF.

26 1 Introduction

27 The study of ion composition in the atmosphere has a long history, and mass spectrometers are being used as an important tool
28 in elucidating their identity and concentrations since the early days. Galactic cosmic rays (GCR) are the main ionisation source
29 in the atmosphere, while radioactive decay (of radon) is more relevant at ground levels. Minor entries originate from lighting,
30 power lines and combustion sources (Curtius, 2006). Higher ion number concentrations are detected in the upper atmosphere
31 and lower number concentrations at ground level. Typically, up to ten thousand ions per cm^3 can be observed within the
32 troposphere owing a life time of a few hundred seconds (Ferguson and Arnold, 1981; Hirsikko et al., 2011). Despite their low



33 abundance, ions can play an important role in atmospheric new particle formation via ion-ion-recombination and ion-induced
34 nucleation (Kirkby et al., 2016) as well as in atmospheric electricity.

35 In the 1970's, F. Arnold and co-workers were the first to study the composition of ions in the lower stratosphere and upper
36 troposphere. In the positive ion spectrum, detected signals were mainly attributed to hydrated hydronium clusters
37 $\text{H}_3\text{O}^+(\text{H}_2\text{O})_{n=1-4}$ and protonated organic vapours (Arnold et al., 1977, 1978). For negative ions, clusters of de-protonated acids
38 like $\text{NO}_3^-(\text{HNO}_3)_m$ and $\text{HSO}_4^-(\text{H}_2\text{SO}_4)_p(\text{HNO}_3)_s$ were identified in the mass range of 1 to 280 amu (Viggiano and Arnold,
39 1981). At ground level, the composition of the main tropospheric ions was also studied by F. Eisele and co-workers with a
40 quadrupole mass spectrometer (Eisele, 1986; Perkins and Eisele, 1984). Using collision-induced dissociation (CID), they
41 identified the 'core' ions of hydrated clusters showing that positive core ions consist mainly of protonated amines. The latter
42 were examined using Tandem-mass spectrometry which helped to identify pyridine and its homologues (Eisele, 1988). Back
43 then, F. Eisele already observed a manifold of tropospheric ions up to 700 amu in the positive ion mass spectrum, but the low
44 mass resolving power of the quadrupole mass analyser was a bottleneck for revealing their sum formula. Tandem mass
45 spectrometry was not performed for these heavy ions for several reasons like insufficient sensitivity and the natural variability
46 (Eisele and Tanner, 1990).

47 The development of an Atmospheric-Pressure interface Time-Of-Flight mass spectrometer (APi-TOF MS, Aerodyne Research
48 Inc. and ToFwerk AG) overcame the limitations of quadrupole mass analysers regarding mass resolving power, duty cycle and
49 mass range. Junninen et al. (2010) demonstrated that this instrument is suitable to detect many unknown ions in the atmosphere
50 and assign sum formulas to many mass peaks for the first time (Ehn et al., 2010; Junninen et al., 2010). Especially in the field
51 of atmospheric new particle formation, the APi-TOF enabled the study of ion formation starting from single molecules such
52 as sulphuric acid, ammonia, amines and highly oxygenated organic molecules (HOM) to the formation of molecular clusters
53 of sizes with a mobility equivalent diameter of 1-2 nm (Almeida et al., 2013; Kirkby et al., 2016; Kürten et al., 2014;
54 Schobesberger et al., 2013). In the last couple of years, the APi-TOF was the key instrument for many scientific studies of new
55 particle formation in both laboratory and field settings (Bianchi et al., 2016; Kirkby et al., 2011; Sipilä et al., 2016).

56 However, questions arose about fragmentation of cluster ions inside the APi-TOF instrument during the ion transfer from
57 ambient pressure through the two quadrupoles and the following lens system to the detector (Ehrhart et al., 2016). It remained
58 unclear if additional ligands besides water molecules might be lost during the ion transfer as well. In a recent publication by
59 Olenius et al. (2013), the authors concluded that fragmentation might be a reasonable explanation for the observed difference
60 in measured and modelled cluster ion distributions of $\text{HSO}_4^-(\text{H}_2\text{SO}_4)_m(\text{NH}_3)_n$ clusters (Olenius et al., 2013).

61 Few publications explicitly studied fragmentation inside the APi-TOF mass spectrometer (Bertram et al., 2011; Brophy and
62 Farmer, 2016; Lopez-Hilfiker et al., 2016). Bertram et al. (2011) showed that fragmentation of cluster ions is strongly sensitive
63 to the voltage settings in the APi. Lopez-Hilfiker et al. (2016) as well as Brophy and Farmer (2016) used two different types
64 of Chemical Ionisation (CI-) APi-TOF to study fragmentation of reagent-adduct-cluster ions. Both found that the electric field
65 inside the APi could be tuned to a low fragmenting "clustered" setting and a high fragmenting "declustering" setting. Even
66 using the low fragmenting setting, however, the transfer of weakly bound cluster ions was evidently affected by fragmentation



67 inside the APi (Brophy and Farmer, 2016; Lopez-Hilfiker et al., 2016). Here, the question arises which cluster bond strengths
68 are how strongly affected by fragmentation.

69 For the instrument configuration used by Lopez-Hilfiker et al. (2016), Iyer et al. (2016) found that for iodide-(I)-chemical
70 ionisation, adduct-molecule clusters with binding energies above 25 kcal/mol are mostly detected with maximum sensitivity
71 at the collisional limit by comparing experimentally measured sensitivities with modelled binding energies. Cluster ions below
72 this threshold suffer from lower sensitivities, likely, due to non-thermal dissociation during the ion transfer inside the mass
73 spectrometer (i.e. partial fragmentation). It remains unclear, if this threshold can be explained by fragmentation in the APi or
74 due to the interactions with the reagent ion in the Ion-Molecule-Region (IMR) of the CI-APi-TOF. In the supplementary,
75 however, the authors conclude that fragmentation in the APi is more reasonable. Furthermore, they also state that cluster ions
76 with binding energies below 10 kcal/mol may not be detectable at all (Iyer et al., 2016). Consequently, there may be two
77 threshold binding energies, one below which partial fragmentation of cluster ions can be expected and the other one below
78 which the non-detection of cluster ions is almost certain. Quantifying these thresholds (e.g. around 10 and 25 kcal/mol for the
79 APi configuration in Iyer et al., 2016) can help characterising the ion transfer of APi-TOF instruments.

80 In those previous studies, the APi's declustering strength was deliberately manipulated by varying the electric potential
81 gradients between two ion optic parts in the APi, e.g. between the skimmer and the second quadrupole (Brophy and Farmer,
82 2016; Lopez-Hilfiker et al., 2016). This electric field is located at the transition from the first to the second pressure stage
83 where the gas pressure drops from two hundred to a few Pa. The cluster ions accelerated by the electrical field can therefore
84 attain relatively high energies via collisions (Zapadinsky et al., 2019, at > 100 Pa, collisions tend to be too frequent and hence
85 low in collision energy, at << 1 Pa, collisions tend to be too rare due to the increased mean free path). Hence, the transition
86 region from the first pressure stage to the second one is also a transition from multi to single collision conditions.

87 The role of the quadrupoles in the fragmentation of cluster ions has not been investigated so far. For multipole ion guides, the
88 number of rods plays a fundamental role regarding their ion transfer properties. The time-averaged radial trapping field within
89 a multipole of 2n electrodes can be well described with the effective potential V^* and gives an idea what to expect for the
90 transfer properties (Gerlich, 1992):

91

$$V^* = \frac{n^2}{4} \frac{q^2}{m\Omega^2} \frac{V_0^2}{r_0^2} \left(\frac{r}{r_0}\right)^{2n-2} \quad (1)$$

92 Here, we have the charge q, the ion mass m, the angular frequency Ω , the amplitude V_0 , the inner radius of the electrode
93 arrangement r_0 and the radial distance of the ion r inside the multipole. The trapping fields of radio-frequency (RF)-only
94 multipoles do not affect the axial kinetic energy of ions (Armentrout, 2000). From Equ. 1, it can be seen that the effective
95 potential of a quadrupole (n=2) varies with $(r/r_0)^2$. On the one hand, this results in an efficient focusing of the ions, but on the
96 other hand, this yields strong perturbations of ions in radial direction and thus, the collision energies are not well defined. Here,
97 a hexapole has a much lower impact on the radial energy due to a larger field free region as its effective potential depends on
98 $(r/r_0)^4$ while still allowing a more pronounced focusing power compared to higher order multipoles. For the same RF settings,



99 a hexapole has a stronger trapping field over quadrupoles of a factor of 9/4 due to the n^2 -dependence of V^* . From this, higher
100 order multipoles should show a lower impact on the stability of cluster ions.

101 Further, it is important to mention the mass discrimination properties of multipole ion guides (Heinritzi et al., 2016). Small
102 ions can be lost due to unstable trajectories at higher RF settings on the multipole, which is known as the low mass cut-off.
103 However, heavy ions typically need a stronger effective potential within the ion guide to be efficiently focused and transferred
104 (see Equ. 1). Therefore, the efficient transmission of small and heavy ions in a multipole ion guide depends on the mass
105 window of the multipole. Higher order multipoles are recommended for the transfer of a broader mass window ranging from
106 low to high masses (Gerlich, 2004). For quadrupole ion guides, the effect of a dramatic cut-off at low masses is especially
107 pronounced due to the much narrower field free region within the quadrupole compared to higher order multipoles (Gerlich,
108 1992). In general, multipoles can be tuned to a mass window of interest. In the field of atmospheric new particle formation, a
109 broad mass range is essential to get a complete understanding of the nucleating ions. Primary ions like NO^+ , O_2^+ or H_3O^+ have
110 different charging properties and the detection of small ions can therefore help to identify the composition of heavy cluster
111 ions by revealing likely ionisation pathways. Thus, information could be lost due to mass discrimination effects for small and
112 heavy ions, respectively. Here, hexapole ion guides show advantageous properties regarding the ion transfer. The properties
113 of multipole ion guides are summarised in Table 1.

114 In the present study, we introduce the ioniAPi-TOF with hexapole ion guides. We characterise the performance of the ioniAPi-
115 TOF regarding ion transmission efficiency, mass range and the impact of electric fields in fragmenting cluster ions.
116 Additionally, we present an inter-comparison with a state-of-the-art quadrupole based APi-TOF during the CERN CLOUD
117 experiment performed in fall 2017 and discuss similarities as well as differences in the instrument's performance.

118 **2 Instrument and methods**

119 **2.1 The ioniAPi-TOF**

120 The ioniAPi-TOF mass spectrometer consists of a laminar flow inlet, an Atmospheric-Pressure interface (APi) including two
121 hexapole ion guides, an ion transfer optic and an orthogonal extraction, reflectron Time-Of-Flight (TOF) mass analyser (see
122 Fig. 1).

123 The laminar flow inlet draws atmospheric ions from the ambient to the inlet of the mass spectrometer via an adjustable flow
124 of 1 to 15 L/min. The inlet is made of a stainless-steel tube with a length of 10 cm and a diameter of $\frac{1}{2}$ " inch. Within this tube,
125 a core-sampling probe is placed in front of the entrance aperture of the ioniAPi-TOF with an inner diameter of 2.5 mm and a
126 length of 25 mm as indicated in Fig. 1.

127 The entrance aperture has a diameter of 0.4 mm yielding an inlet flow of 1.1 L/min from ambient pressure into the mass
128 spectrometer. Skimmers with bore diameters of 1.2 mm separate the different pressure stages. Two hexapole ion guides of the
129 same length are installed in the first and second pressure stage of the Atmospheric-Pressure interface. The first hexapole is
130 running at a frequency of 1 MHz and an amplitude of 200 V_{pp} . The frequency of the second hexapole is about 5.5 MHz with



131 an amplitude of 600 V_{pp}. The third pressure stage contains an ion transfer optical lens system consisting of two lens stacks. It
132 focuses the ion beam coming from the hexapoles and transfers it to the orthogonal extraction region of the mass spectrometer.
133 As Time-Of-Flight mass analyser, we chose the ioniTOF1000 platform of IONICON Analytik GmbH (Innsbruck, Austria). It
134 is a compact Time-Of-Flight mass spectrometer with a short ion flight path of roughly 0.5 m and therefore expected to have a
135 sufficiently high ion transmission efficiency, which is important due to the low abundance of atmospheric ions. The same
136 Time-of-Flight mass analyser was already presented in Müller et al., (2014). The ioniTOF1000 is made of a multistage
137 orthogonal-extraction region consisting of a pusher and four mesh electrodes supplied with a reference, pull, grid as well as a
138 drift tube cage voltage.

139 Depending on the desired mass range of interest, the extraction frequency can be adjusted to measure ions of a mass-to-charge
140 (m/z) ratio of up to 10,000 Th (1 Thomson = 1 Da/e⁻). For the results presented herein, the extraction frequency is typically set
141 to 30 kHz to measure ions up to 2,000 Th.

142 A double-stage reflectron is used for an improved mass resolution leading to a V-shaped ion flight path. Ions are post-
143 accelerated and detected with a multichannel plate (MCP) stack with a voltage of ~2200 V. Compared to Müller et al. (2014)
144 we achieved a mass resolution at full-width half maximum (FWHM) of ~2000 for ions above m/z 100, see Fig. 3.

145 A Hyco 4-cylinder diaphragm pump is used at ambient pressure to draw air through the laminar flow inlet. A Pfeiffer Vacuum
146 ACP 40 roots pump is used as fore pressure pump to reduce the pressure in the cell of the first hexapole in the ioniAPI-TOF
147 to 2.3 mbar. Three Pfeiffer Vacuum HiPace 80 turbo-molecular pumps, which are connected to a MD1 diaphragm pump of
148 Vacuubrand, evacuate the ion transfer optics region and the TOF mass analyser. Together they maintain a typical pressure of
149 a few 10⁻³ mbar in the second hexapole of the ioniAPI, followed by 10⁻⁴ mbar within the lens stacks and a few 10⁻⁶ mbar in the
150 TOF mass analyser.

151 As described in Müller et al. (2014) a time-to-digital converter (TDC) is used to convert the MCP signals into ion counts per
152 time-bin. The applied extraction frequency of 30 kHz results in about 280,000-time bins. The IONICON TOF 3.0 software is
153 used for data acquisition. The data is stored in the HDF5-file format (HDF5-group). The ioniAPI-TOF allows detection of ions
154 in positive and negative ion mode. In this work, we present results of the positive ion mode only.

155 2.2 Cluster Calibration Unit

156 The Cluster Calibration Unit (CCU) allows the calibration of the mass-axis over a broad mass range and of the mass-dependent
157 transmission efficiency of (CI-)API-TOF mass spectrometers (Heinritzi et al., 2016). For this purpose, the CCU consists of an
158 electrospray ionisation source (ESI), a “Vienna”-type high-resolution Differential Mobility Analyser (UDMA, Steiner et al.,
159 2010) and a Faraday-Cup electrometer (FCE, Winklmayr et al., 1991); see Fig. 2.

160 Millimolar solutions of tetra-alkyl-ammonium halides dissolved in acetonitrile are used for the ESI, see Table 2 for details
161 (Ude and Fernández de la Mora, 2005). By applying a high voltage of a few kV, the ESI generates cluster ions of the desired
162 polarity. A transport flow of typical 14 L/min transfers the ions over a distance of a few centimetres from the ESI directly into
163 the UDMA. Within the UDMA, the ions are classified in terms of their electrical mobility. In this study, a filtered recirculating



164 sheath flow of about 700 L/min was used. Under these conditions and the given geometry, the resolving power of the UDMA
165 was around 10 to 15, which is sufficient to distinguish ionic monomers, dimers and trimers of one selected calibration
166 compound within the ion mobility spectrum. For details on the definition on the resolving power of DMAs we refer to Flagan,
167 1998.

168 To retrieve the transmission at a desired mass-to-charge (m/z) ratio in the mass spectrometer, the UDMA can be set to a
169 constant voltage that corresponds to a specific electrical mobility. Consequently, only ions of the corresponding electrical
170 mobility will pass the UDMA. The aerosol flow coming from the outlet of the UDMA is guided through an 8 mm stainless
171 steel tube of 10 cm length. After this length, the flow is separated via a Y-shaped flow splitter with an angle of 40° between
172 the two outlet tubes to reduce inhomogeneities of the sample flow. For the same reason, the flow rates to both the FCE and the
173 ioniAPI-TOF are set equally.

174 2.3 Experiments with a corona ion source

175 For the comparison of a low fragmenting (clustered) setting (voltage difference: $dV = -1.4$ V) and a high fragmenting
176 (declustering) setting (voltage difference: $dV = -10.0$ V) described in chapter 3.2, ions were generated with a corona ion source.
177 A $\frac{1}{2}$ " T-piece was connected to the $\frac{1}{2}$ " laminar flow inlet in front of the ioniAPI-TOF. Lab air was drawn in a straight line
178 through the T-piece. The corona needle was placed through a $\frac{1}{2}$ " plug into the T-piece orthogonally to the flow direction. The
179 needle tip was sitting below the air flow.

180 A voltage of +1.7 kV lead to the ionisation of ambient air streaming into the direction of the entrance aperture of the mass
181 spectrometer. Hereby, a large variety of ions was produced via ion-molecule reactions and charge transfer covering a mass
182 range from 18 to 1000 Th. The reaction time within the laminar flow inlet was approximately 35 ms. In the course of the
183 experiment, high amounts of $H_3O^+(H_2O)_n$ were needed to study the fragmentation of these cluster ions. The corona ion source
184 yielded sufficient and stable ion signals for constant flow conditions inside the inlet tube as will be shown in chapter 3.2, Fig.
185 7.

186 2.4 CLOUD experiment

187 To test the performance of the ioniAPI-TOF under the high-demanding conditions of a long-term measurement campaign with
188 the challenge of various experimental conditions and different chemical systems, we participated in the CLOUD 12 campaign
189 in fall 2017. The CLOUD (Cosmics Leaving OUTdoor Droplets) experiment at the European Centre for Nuclear Research
190 (CERN) studies the influence of galactic cosmic rays (GCR) on atmospheric new particle formation under very well-controlled
191 conditions (Duplissy et al., 2016; Kirkby et al., 2011). This effect can be studied by comparing the experiments at ground level
192 GCR ion pair production rates to experiments under neutral conditions inside the chamber where a high voltage field is turned
193 on. Upper tropospheric ion pair production rates and ion number concentrations can be realised via a π -beam of 3.5 GeV/c
194 from the CERN Proton Synchrotron. The chamber is made of electro-polished stainless steel with a volume of 26.1 m³. At the
195 top and at the bottom of the chamber, two fans made of stainless steel are used for homogeneous mixing of the air yielding



196 mixing times of a few minutes. To study a wide range of tropospheric conditions, a thermal housing allows experiments at
197 temperatures ranging from 203 to 310 K with a stability of 0.1 K. A very clean atmosphere is obtained using cryogenic N₂ and
198 O₂ in the natural ratio of 79:21 with a level of contaminant vapours in the sub-ppt_v range (Schnitzhofer et al., 2014). The effect
199 of relative humidity can be studied by adjusting the flow rate of ultrapure de-ionized water being vaporised into the chamber.
200 Ozone is produced via UV photolysis of O₂. The volume-mixing ratio of O₃ can be controlled by the flow rate. Further trace
201 gases like SO₂, NH₃, isoprene (C₅H₈) or α -pinene (C₁₀H₁₆) can be introduced separately via a gas handling system.
202 During the measurements at the CLOUD experiments, we used a critical orifice at the exhaust of the inlet to maintain a constant
203 flow rate of 12.6 L/min as this was found to be the optimal setting regarding the total ion signal intensity. The ioniAPi-TOF
204 inlet line was connected via a flow splitter with the PTR3 (Breitenlechner et al., 2017) to the same CLOUD sampling port.
205 Due to reasons of limited space around the CLOUD chamber, the ioniAPi-TOF was mounted on top of the PTR3.
206 Consequently, it could not be connected via a straight line to the flow splitter. We connected the instrument with two 30 cm
207 long flexible well tubes and one additional straight tube. All tubes were made of stainless steel. In total, the sigmoidal-shaped
208 inlet line to the flow splitter had a length of 1.2 m. Together with the length of the sampling probe that reached into the
209 chamber; the total length of the inlet line was about 1.95 m and had a diameter of 1/2". Besides wall losses due to the length of
210 the inlet line, the flexible well tubes might have resulted in an additional loss factor due to their rippled inner surface.

211 2.5 The APi-TOF

212 The operation principle of the APi-TOF of the University of Eastern Finland (UEF) is similar to what has been extensively
213 reported in previous publications (Junninen et al., 2010; Schobesberger et al., 2013). The instrument was directly connected
214 to the CLOUD chamber through a 30 cm long stainless-steel tubing with an outer diameter of 1" (25.4 mm), which was then
215 reduced to 10 mm diameter in the last 10 cm of the tubing. The flow rate inside the sampling tube was in total 9 L/min all the
216 way to the 0.3 mm diameter sampling pinhole of the instrument. From the 9 L/min total flow, 0.8 L/min entered the instrument.
217 The UEF APi-TOF was operated in positive ion mode for the experiments shown here with ion guiding quadrupoles operating
218 at pre-defined "high mass" settings having a mass range of about 100 – 2000 m/z.

219 The main differences in the configuration of both instruments are listed in Table 3. The configuration of the ion transfer system
220 in the APi shows major differences due to the use of segmented quadrupoles in the UEF APi-TOF while non-segmented
221 hexapoles are used in the ioniAPi-TOF as well as other geometric factors like e.g. skimmer orifice diameters and distances.
222 The different lengths of the TOF mass analysers explain differences in the mass resolving power and the extraction frequencies.

223 2.5 Data analysis and post-processing

224 The data of the UEF APi-TOF were processed using the MatLab based tofTools package Version 6.11 (Junninen et al., 2010).
225 We used the Ionicon PTR-MS Viewer 3.2 and TOF data processing scripts written by Lukas Fischer for data analysis of the
226 UIBK ioniAPi-TOF (for TOF data processing scripts see Breitenlechner et al., 2017).



227 3 Results

228 3.1 Characterisation of the transmission efficiency

229 The overall absolute transmission efficiency of the ioniAPi-TOF was determined with the Cluster Calibration Unit for a mass
230 range of 74 to 1640 Th. The transmission efficiency of a selected m/z was determined by the ratio of ion count rates measured
231 with the ioniAPi-TOF and the FCE. The substances listed in Table 2 were used as calibration standards. Monomer, dimer,
232 trimer and tetramer cluster ions were produced with the ESI and selected each as a monodisperse aerosol via the UDMA. The
233 smallest ion was the monomer of tetra-methyl-ammonium iodide at m/z 74 and the heaviest cluster ion used was the tetramer
234 of the ionic liquid with m/z 1640.

235 The mass spectrum of a monodisperse aerosol typically has major counts at the m/z peak of the mobility selected ion. Minor
236 counts of ions of $m/z < 100$ like O_2^+ , $H_3O^+(H_2O)_{n=0-3}$, $NH_4^+(H_2O)_{n=0-2}$ as well as protonated acetonitrile clusters $H^+(C_2H_3N)_{1-2}$
237 were also observed. Additionally, minor peaks of impurities or fragments were observed. In the case of dimers, their signal
238 still showed the highest intensity. In addition, a peak at the m/z of the monomer appeared with a relative abundance of less
239 than 10 %. The observation of fragments was even more pronounced in the case of trimers. Here, the signals of monomers and
240 dimers reached in some cases similar intensities compared to the trimer, although only the trimer was expected.

241 This was not only observed for all mobility standards in Table 2, but also in different types of APi-TOF mass spectrometers
242 using the CCU. We could observe the same fragmentation pattern with the ioniAPi-TOF as well as with the UEF APi-TOF in
243 the course of the inter-comparison, and also with an H-TOF, Tofwerk AG Thun Switzerland, without an APi interface in the
244 laboratory at the University of Innsbruck (UIBK). To our knowledge, there exist only a few detailed reports of observations
245 of such fragmentation patterns for the standards we used here. Heinritzi et al. (2016) reported fragmentation of iodide dimers
246 in the negative ion mode. While Junninen et al. (2010) did not observe such fragmentation with the calibration standards, only
247 at a mobility diameter of 1.6 nm a fragment possibly due to an impurity was reported.

248 The observation of peaks at the monomer and dimer masses for selected ion mobilities of trimers can either be interpreted as
249 fragments or as the result of a broad tail of the UDMA's transfer function allowing ions of high abundance to be still partially
250 transferred despite not having the expected ion mobility. Further, also multiply charged ions with the same ion mobility could
251 pass the UDMA and evaporate or fragment afterwards leading to the formation of monomers and dimers which are then
252 detected (Rus et al., 2010). No peaks of multiply charged ions were observed in the mass spectrum. So far, we exclude
253 fragmentation inside the ioniAPi as explanation, as we will show in section 3.2. that, when using the low fragmenting setting
254 in the ioniAPi (voltage difference: -1.4 V) the cluster ion $H_3O^+(H_2O)_3$ does not appear to fragment almost at all, even though
255 it is relatively weakly bound (binding energy: $BE(H_3O^+(H_2O)_3) = -\Delta H = 17$ kcal/mol, (Meot-Ner, 1984)). For much heavier
256 cluster ions, such as produced with the calibration standards, even higher collision energies would be necessary for a
257 fragmentation of the observed intensity. The relationship between the energy in the lab system E_{lab} and the centre-of-mass
258 energy E_{CM} is shown in Equ. 2 (Armentrout, 2002). Here, m is the mass of the buffer gas (air) and m_{ion} the mass of the ion.



259 E_{CM} is proportional to the reciprocal of the ions' mass m_{ion} . With increasing mass, higher electric fields would be necessary to
260 reach sufficient collision energies for heavy ions.

$$261 \quad E_{CM} = \frac{m}{m+m_{ion}} \cdot E_{lab} \quad (2)$$

262 The conversion into the centre-of-mass frame of reference allows the estimation that for ions with a high m/z , e.g. $m/z > 250$
263 Th, the collision energy under low fragmenting settings and air molecules as buffer gas should not be sufficient to explain the
264 observed peak pattern by fragmentation.

265 However, the fractions of fragment signals can be corrected as done in Heinritzi et al. (2016). For this purpose, we assume that
266 the fragmentation occurs outside the APi. Thus, the electrometer counts the fragments as well. In general, ions of different m/z
267 have different transmission efficiencies through an APi. To obtain the transmission of the monomer, solely the sum of count
268 rates at the monomer mass and its isotope peaks was divided by the expected count rate that was determined from the current
269 measured with the electrometer. With the obtained monomer transmission efficiency, the electrometer signal was corrected to
270 determine the transmission for the dimer. Further, the transmission factor of the monomer and the corrected transmission factor
271 of the dimer were used to determine the transmission of the trimer.

272 In the end, this leads to the overall absolute transmission efficiency shown in Fig. 4. An overall transmission efficiency of
273 about 1 % was found. Taking the instruments background noise into account, this corresponds to a detection limit of roughly
274 $5 \cdot 10^{-3}$ ions/cm³ for 5-min integration time and $5 \cdot 10^{-4}$ ions/cm³ for one-hour integration time. The error in determining the
275 transmission efficiency due to fragment peaks was found to be less than 10 %. In general, the transmission is highest in the
276 mass range from 200 to 600 Th and decreases for heavier ions. The transmission of small ions was only determined in the
277 course of one experiment where it seems to decrease sharply to values as low as for heavy ions. Nevertheless, we later observed
278 the highest individual ion count rates are under standard (low fragmenting) settings highest at ions below m/z 100 (for example
279 see Fig. 9). This may indicate that small natural ions are more than one order of magnitude more abundant than heavier ions
280 or that the transmission at m/z 74 is underestimated.

281 The transmission efficiency was determined for both the low fragmenting (voltage difference: $dV = -1.4$ V) and the high
282 fragmenting (voltage difference: $dV = -10.0$ V) setting for comparison. As shown in Fig. 4, the low-fragmenting setting yields
283 a higher transmission efficiency for most of the mass range. Despite an overall lower transmission, the high-fragmenting setting
284 offers a slightly higher transmission for heavier ions, here m/z 1391, due to the better focusing of heavier ions. This resembles
285 a shift or a tilting of the transferred mass window. Overall, though, both settings offer a comparable high ion transmission.
286 The data points (Fig. 4) determined after the CLOUD campaign for the low fragmenting setting are comparable to the
287 calibration done in the beginning of the campaign.

288 3.2 Characterisation of the ion transfer

289 In the following, we address the question of fragmentation inside the ioniAPi-TOF. As mentioned in the introduction, recent
290 studies demonstrated that the electric potential difference between parts of the ion optics in the APi can be used to study



291 collision induced fragmentation of cluster ions, e.g. a voltage difference dV between the skimmer and the second multipole
292 (Brophy and Farmer, 2016; Lopez-Hilfiker et al., 2016).

293

294 3.2.1 Low and high fragmenting setting

295 To compare the afore-mentioned low and high fragmenting settings, hydrated hydronium clusters ($H_3O^+(H_2O)_{n=0-3}$) were used
296 as a model system due to their well-known binding energies, see Table 4 (Meot-Ner, 1984). In Fig. 5, the distribution of the
297 hydrated hydronium clusters is exemplarily shown for both settings. Ions were produced using a corona ion source in front of
298 the inlet as introduced in chapter 2.3. We used the fits of the ion transmission efficiency of the low and the high fragmenting
299 setting from Fig. 4 to correct the individual ion intensities for all the water-clusters with respect to transmission effects.

300 In the low fragmenting setting, the higher order and weakly bound hydrated hydronium clusters $H_3O^+(H_2O)_2$ and $H_3O^+(H_2O)_3$
301 show the highest abundance (Fig. 5). The high fragmenting setting (highest dV) overall leads to the cluster distribution shifting
302 to smaller and more strongly bound hydrated hydronium clusters, $H_3O^+(H_2O)_3$ largely dissociates, thereby reducing its intensity
303 by a factor of 10.

304 The peak at m/z 91.06, assumed to be $H_3O^+(H_2O)_4$, is also included in the figure. Its signal intensity seems to behave as
305 expected for the low and the high fragmenting setting because it shows a reduction for the latter setting.

306 The intensity of H_3O^+ increased by a factor of 25 for the high fragmenting setting. Although this is a significant increase, the
307 new cluster equilibrium ends with $H_3O^+(H_2O)$ and $H_3O^+(H_2O)_2$ showing the highest intensities. Evidently, a voltage difference
308 of -10 V which was the maximum adjustable voltage setting is not enough to completely fragment $H_3O^+(H_2O)$ cluster ions
309 (bound most strongly, $-\Delta H = 31.5$ kcal/mol; Table 4).

310

311 3.2.2 Declustering scan

312 A so-called declustering scan investigates the relation of voltage settings in the API to the binding energy of cluster ions
313 (Lopez-Hilfiker et al., 2016). In analogy to that study, the voltage difference between skimmer-1 and the second hexapole was
314 stepwise increased, here by changing the DC offset of the hexapole (Fig. 6). The ion optics following the second hexapole
315 were set to one setting during the declustering scan to maintain a high transmission efficiency. The declustering scan started
316 from $dV = 0$ V to -10 V in steps of 1 V, skimmer-1 being grounded. Ions were generated with a corona ion source as before.

317 Each increase in dV results in a higher collision energy. This explains why primarily the higher order hydrated hydronium
318 clusters show a decrease for the lowest voltage steps. First, $H_3O^+(H_2O)_3$ is collisionally fragmenting due to its low binding
319 energy ($-\Delta H = 17$ kcal/mol, see Table 4). In the centre-of-mass system, the collision energy needed to break the cluster bond
320 corresponds to the Gibbs free energy of the $H_3O^+(H_2O)_3$ cluster ($\Delta G = -9$ kcal/mol at 298 K, see Table 4). Although the Gibbs
321 free energy is more accurate in describing the energy of a cluster ion within this process, the estimation of the Gibbs free
322 energy is not straightforward. This is due to the uncertainty of temperature in the transition from the first to the second pressure
323 stage. Therefore, we exemplarily determined the ΔG -values for the hydrated hydronium clusters at a temperature of 298 K in
324 Table 4. In the following, we use the binding energy ($-\Delta H$).



325 Further increase of dV results in the fragmentation of $H_3O^+(H_2O)_2$ which has a slightly higher binding energy ($-\Delta H = 20$
326 kcal/mol). While larger clusters are fragmenting an increase is observed for $H_3O^+(H_2O)$. Above a dV of -9 V, also the intensity
327 of $H_3O^+(H_2O)$ starts to show a decrease. Here, the collision energy is already high enough to partially fragment $H_3O^+(H_2O)$
328 that has a much higher binding energy ($-\Delta H = 31.5$ kcal/mol). H_3O^+ shows a steady increase which is pronounced for higher
329 dV .

330 Lopez-Hilfiker et al. (2016) found a linear relationship between the dV_{50} of an iodide-CI-APi-TOF and the binding energy
331 (Lopez-Hilfiker et al., 2016). In accordance to that study, we used a non-linear least square sigmoidal model to fit the data
332 points. From the fit we determined the characteristic voltage at half maximum (dV_{50}) of -5.6 and -7.5 V for $H_3O^+(H_2O)_3$ and
333 $H_3O^+(H_2O)_2$, respectively. The higher dV_{50} obtained for $H_3O^+(H_2O)_2$ is consistent with its binding energy being higher than
334 the one of $H_3O^+(H_2O)_3$ (see Table 4).

335

336 3.2.3 Threshold binding energies

337 The results from section 3.2.2 allow establishing an approximate threshold cluster binding energy for a fragment-free transfer
338 through the mass spectrometer. To estimate this threshold for the ioniAPi-TOF, we start with the $H_3O^+(H_2O)_3$ cluster ion. From
339 the declustering scan in Fig. 7, the decrease of the ion signal of $H_3O^+(H_2O)_3$ starts at a voltage difference (dV) of -3 to -4 V.
340 The low fragmenting setting typically is set to a dV of -1.4 V. Therefore, we conservatively estimate that cluster ions with
341 binding energies above 17 kcal/mol are likely to be transferred through the ioniAPi without substantial fragmentation for the
342 low fragmenting setting. Cluster ions with binding energies below this threshold are partially affected by fragmentation with
343 increasing degree. Assuming a linear relationship between the voltage difference and the binding energy, we extrapolate a
344 threshold binding energy of 8 to 10 kcal/mol below which cluster ions are not likely to be detected depending on other
345 conditions in the ioniAPi.

346 To compare the threshold binding energy of fragment-free cluster transfer of the ioniAPi-TOF to a quadrupole based APi-
347 TOF, we only can give rough estimates based on existing literature. Via comparing modelled binding energies for adduct
348 cluster ions and their sensitivity with a CI-APi-TOF, Iyer et al. (2016) estimated that cluster ions with a binding energy below
349 25 kcal/mol can be expected to fragment at least partially during the ion transfer for the CI-APi-TOF in Lopez-Hilfiker et al.
350 (2016) and that cluster ions of binding energies below 10 kcal/mol are not likely to survive the transfer. Although it is not clear
351 from their study if fragmentation can happen in the IMR or in the APi of the instrument, they conclude in the supplementary
352 that fragmentation in the APi is more likely (Iyer et al., 2016).

353 In Brophy and Farmer (2016), a declustering (dV) scan of the acetate-acetic acid cluster ($C_2H_3O_2^-(C_2H_4O_2)$) is shown. The
354 voltage difference was also scanned between the skimmer and the front of the second multipole as done in this study (Fig. 4
355 in Brophy and Farmer). For this region, the authors determined a dV_{50} of 4.1 V for $C_2H_3O_2^-(C_2H_4O_2)$ which has a binding
356 energy of 29.3 kcal/mol (Meot-Ner and Sieck, 1986). At a voltage difference of 0 V, this cluster did not completely reach a
357 plateau which must be considered as still partially fragmenting. From this, the threshold binding energy for their instrument
358 seems to be even above the CI-APi-TOF in Iyer et al. (2016). In contrast, Bertram et al. (2011) showed a mass spectrum of



359 acetate-acetic acid cluster ions where under weak electric fields (15 V/cm throughout the APi) also higher order clusters
360 ($C_2H_3O_2^-(C_2H_4O_2)_{1-2}$) were detectable with their CI-APi-TOF instrument (Bertram et al., 2011). The binding energy of the
361 trimer ($C_2H_3O_2^-(C_2H_4O_2)_2$) is 19.6 kcal/mol (Meot-Ner and Sieck, 1986). From Bertram et al. (2016), also a lower fragmenting
362 transfer of cluster ions for a quadrupole based APi-TOF is possible. While no quantitative threshold binding energy was
363 determined, it can only be estimated to be in the order of the binding energy of the acetate-acetic acid trimer of 19.6 kcal/mol.
364 The differences in thresholds of fragment-free cluster transfer for the mentioned instruments depend obviously on more factors
365 than the applied voltage settings in the APi like instrument geometry, pressures and flows. Nevertheless, our data suggests that
366 the ioniAPi allows a slightly lower threshold binding energy for the transfer of cluster ions. From our data, it is still difficult
367 to attribute the observed difference to the number of poles of the ion guides. In the case of RF-only ion guides, this difference
368 could be explained only by the radial contribution of the multipoles. Here, more research is needed regarding the effect of RF-
369 frequency and amplitude on cluster ions at different pressures. For example, Rus et al. (2010) concluded that RF heating in the
370 multipole was responsible for fragmentation of unstable cluster ions. Further, the successful fragmentation of a cluster via a
371 collision with air as buffer gas depends also on the achieved collision energy in the centre-of-mass system. Heavier ions need
372 higher electric fields to achieve the necessary collision energy. But they also can more readily accumulate the collision energy
373 in a higher number of vibrational modes within the cluster compared to smaller ions reducing their chance of fragmentation
374 (Zapadinsky et al., 2019).

375

376 3.3 Mass window and comparison to a quadrupole based APi-TOF MS

377 In the course of the CLOUD 12 campaign, we conducted an inter-comparison with the quadrupole based APi-TOF mass
378 spectrometer of the University of Eastern Finland (UEF). The results of the transmission efficiency inter-comparison in
379 positive ion mode made at the end of the campaign are shown in Fig. 8. The data points are corrected for cluster fragments as
380 mentioned in chapter 3.1. Here, inlet line losses are not accounted for as the calibration setup of the CCU allows nearly identical
381 flow conditions for both detectors, electrometer and mass spectrometer. A transmission efficiency of overall about 1% was
382 found for both mass spectrometers. The overall ion transmission is a factor of 2 to 3 higher for the UEF APi-TOF. This factor
383 can be attributed to various differences in the instrument configurations as described in section 2.5, e.g. ion optic configuration,
384 geometry as well as flows due to pumping. It can be noted that due to the compact size of the TOF mass analyser of the
385 ioniAPi-TOF, it can be run at a higher duty cycle with an almost threefold higher extraction frequency. Due to the higher
386 extraction, more ions are detected leading to a comparable transmission efficiency with the UEF APi-TOF.

387 From Fig. 8, the UEF APi-TOF has a higher transmission for medium mass ions between 200 and 600 Th. At higher masses
388 at about 1000 Th, the difference in the transmission efficiency of both instruments decreases. This can be explained with the
389 different ion transfer properties of higher order multipoles as shown in Table 1. In general, hexapole ion guides allow a poorer



390 focusing compared to quadrupoles but are capable of transmitting a broader mass range. Examples below will demonstrate
391 these properties using parallel measurements.

392 A qualitative inter-comparison was performed during a CLOUD experiment at CERN where the ozonolysis of a mixture of α -
393 pinene and isoprene was studied at $-50\text{ }^{\circ}\text{C}$. The experimental conditions for the inter-comparison of both APi-TOF instruments
394 are noted in Table 5. This experiment was chosen because oxidation of α -pinene is expected to form highly oxygenated
395 molecules (HOM) (Ehn et al., 2010; Kirkby et al., 2016) and therefore high mass ions. Another reason was the use of the
396 CERN π -beam, which yields increased ion concentrations inside the CLOUD chamber leading to higher ion count rates with
397 both APi-TOFs and a better signal to noise ratio (S/N). The mass spectra obtained by the ioniAPi-TOF and the UEF APi-TOF
398 are compared in Fig. 9. Ion count rates are corrected for diffusion losses with the Gormley-Kennedy equation (Bemgård et al.,
399 1996) for both instruments.

400 First, this inter-comparison shows that in general, the overall peak pattern for the experiment is comparable for both
401 instruments. Several “bands” consisting of combinations of C5- and C10 HOM appear in both mass spectra and show a similar
402 distribution, e.g. mass ranges 300 to 450 Th, 450 to 650 Th, 650 to 850 Th and 850 to 1050 Th. For example, the peaks at m/z
403 151, 153, 169 and 185 correspond to $\text{C}_{10}\text{H}_{15}\text{O}^+$, $\text{C}_{10}\text{H}_{17}\text{O}^+$, $\text{C}_{10}\text{H}_{17}\text{O}_2^+$ and $\text{C}_{10}\text{H}_{17}\text{O}_3^+$, respectively showing the same relative
404 intensity in the mass spectrum of the ioniAPi-TOF as well as in the APi-TOF. Further analysis of the mass spectral data is not
405 subject to the present study.

406 Secondly, comparing the peak intensities a difference in the dynamic range between both instruments, the UEF APi-TOF and
407 the UIBK ioniAPi-TOF, for ions above a m/z of roughly 350 can be seen. This can mainly be attributed to the differences in
408 mass resolution (for this experiment, ~ 5000 (APi-TOF) and ~ 1600 (ioniAPi-TOF)) leading to a higher dynamic range for the
409 UEF APi-TOF. Higher diffusion losses in the much longer inlet line during the experiment as well as differences in the ion
410 transmission efficiency (see Fig. 8) can additionally contribute to the lower dynamic range of the ioniAPi-TOF.

411 Thirdly, the mass spectra show large differences for ions of masses below 100 Th. As the UEF APi-TOF is set to the high
412 mass range setting, the high-pass mass filter property of the quadrupole leads to the low-mass cut-off disabling the detection
413 of small ions in exchange for an increase in ion transfer and detection of high mass ions. The use of hexapoles as ion guides
414 in the ioniAPi-TOF allows the detection of small ions below m/z 100 and of high mass ions up to 1100 Th simultaneously as
415 shown for the tested experimental conditions. Here, only the mass range up to 1100 Th is shown as ion count rates at higher
416 m/z were too low in both instruments, setting a practical upper m/z limit for this comparison.

417 However, the calibration results shown in Fig. 8 suggest that both instruments have a comparable level of transmission
418 efficiency for ions above 100 Th. From this perspective, the hexapole ion guides show beneficial properties when measuring
419 a broad mass range. The loss of information on one end of the mass window, as evident here for the quadrupole system, is not
420 necessary. We note that this effect is not exclusively limited to comparing hexapole with quadrupole systems, as progression
421 to even higher order multipoles may further broaden the accessible mass range. However, this will be subject to a future study.



422 4 Conclusion

423 In the present study, we introduce an alternative type of Atmospheric Pressure-interface Time-Of-Flight mass spectrometer,
424 the so-called ioniAPiTOF, with the main difference of using hexapoles as ion guides in the APi. We characterised the ioniAPi-
425 TOF regarding ion transmission efficiency, mass range transmission and the effect of ion transfer properties on the cluster ion
426 stability. We found that the overall ion transmission efficiency (so far tested from m/z 74 to 1640 Th) with hexapole ion guides
427 is around 1 % and comparable to existing APi-technology using quadrupole ion guides. The detection limit for one-hour
428 integration time is around $5 \cdot 10^{-4}$ ions/cm³. The width of the transmitted mass range was found to be broader compared to a
429 quadrupole based APi-TOF, when each instrument was using just one single setting. In atmospheric nucleation studies, this
430 has the advantage of simultaneously detecting very small precursor ions, which can harbour information on nucleation
431 precursor compounds, and the much heavier cluster ions that form during nucleation. Further, the effect of the ion transfer
432 through the ioniAPi on the cluster stability and their fragmentation was studied. Using the system of $H_3O^+(H_2O)_n$ we were able
433 to estimate that cluster ions with binding energies above 17 kcal/mol are not substantially fragmenting. From the literature, we
434 estimated a threshold of roughly 20 to 25 kcal/mol for quadrupole based APi-TOF instruments. Comparing these numbers, a
435 slightly less fragmenting ion transfer for the ioniAPi seems possible. Still, further work is needed to understand the differences
436 in fragmentation inside various APi configurations and if the lower fragmenting transfer suggested for the ioniAPi is due to
437 the number of poles or if other differences (e.g. pumping, geometry, voltage settings) are responsible. The mass resolution of
438 ~ 2000 in the present study was limited by the use of a compact TOF mass analyser. Future focus lies on improving both mass
439 resolution and the transmission efficiency.

440

441 *Data availability.* Data related to this article are available on request from the corresponding authors.

442

443 *Author contributions.* PM, SF, GS and ML did the measurements with the ioniAPi-TOF in Innsbruck while GS and ML
444 performed the measurements at the CLOUD experiment. ML did the data analysis of the ioniAPi-TOF experiments. AY
445 contributed with data obtained with the UEF API-TOF at the CLOUD experiment. ML wrote the manuscript and all authors
446 contributed to the final manuscript development.

447

448 *Acknowledgements.* We thank IONICON Analytik GmbH for providing an ioniTOF-1000 mass spectrometer and for the
449 support in the development of the ioniAPi-TOF MS. Furthermore, we thank CERN for support of the CLOUD experiment as
450 well as the CLOUD collaboration (www.cern.ch/cloud) for the opportunity to test the new instrument and for their support.
451 We thank the tofTools team for providing tools for mass spectrometry analysis.

452

453 *Funding.* This work is funded by the Austrian Science Fund, FWF (project no. P27295-N20), the Tiroler Wissenschaftsfonds
454 (nanoTOF-ICE), the University of Innsbruck promotion grant for young researchers, the Academy of Finland's Centre of



455 Excellence program (grant no. 307331) and the University of Eastern Finland Doctoral Program in Environmental Physics,
456 Health and Biology.

457

458 *Competing financial interests.* The authors declare the following competing financial interest: IONICON Analytik GmbH
459 plans to commercialise the ioniAPi-TOF.

460 References

- 461 Almeida, J., Schobesberger, S., Kürten, A., Ortega, I. K., Kupiainen-Määttä, O., Praplan, A. P., Adamov, A., Amorim, A.,
462 Bianchi, F., Breitenlechner, M., David, A., Dommen, J., Donahue, N. M., Downard, A., Dunne, E., Duplissy, J., Ehrhart, S.,
463 Flagan, R. C., Franchin, A., Guida, R., Hakala, J., Hansel, A., Heinritzi, M., Henschel, H., Jokinen, T., Junninen, H., Kajos,
464 M., Kangasluoma, J., Keskinen, H., Kupc, A., Kurtén, T., Kvashin, A. N., Laaksonen, A., Lehtipalo, K., Leiminger, M.,
465 Leppä, J., Loukonen, V., Makhmutov, V., Mathot, S., McGrath, M. J., Nieminen, T., Olenius, T., Onnela, A., Petäjä, T.,
466 Riccobono, F., Riipinen, I., Rissanen, M., Rondo, L., Ruuskanen, T., Santos, F. D., Sarnela, N., Schallhart, S., Schnitzhofer,
467 R., Seinfeld, J. H., Simon, M., Sipilä, M., Stozhkov, Y., Stratmann, F., Tomé, A., Tröstl, J., Tsagkogeorgas, G., Vaattovaara,
468 P., Viisanen, Y., Virtanen, A., Vrtala, A., Wagner, P. E., Weingartner, E., Wex, H., Williamson, C., Wimmer, D., Ye, P.,
469 Yli-Juuti, T., Carslaw, K. S., Kulmala, M., Curtius, J., Baltensperger, U., Worsnop, D. R., Vehkamäki, H. and Kirkby, J.:
470 Molecular understanding of sulphuric acid-amine particle nucleation in the atmosphere, *Nature*, 502(7471), 359–363,
471 doi:10.1038/nature12663, 2013.
- 472 Armentrout, P. B.: Kinetic energy dependence of ion-molecule reactions: Guided ion beams and threshold measurements,
473 *Int. J. Mass Spectrom.*, 200(1–3), 219–241, doi:10.1016/S1387-3806(00)00310-9, 2000.
- 474 Armentrout, P. B.: Mass spectrometry - Not just a structural tool: The use of guided ion beam tandem mass spectrometry to
475 determine thermochemistry, *J. Am. Soc. Mass Spectrom.*, 13(5), 419–434, doi:10.1016/S1044-0305(02)00347-1, 2002.
- 476 Arnold, F., Krankowsky, D. and Marien, K. H.: First mass spectrometric Measurements of Positive Ions in the Stratosphere,
477 *Nature*, 267(5), 30–32, 1977.
- 478 Arnold, F., Böhringer, H. and Henschen, G.: Composition measurements of stratospheric positive ions, *Geophys. Res. Lett.*,
479 5(8), 653–656, doi:10.1029/GL005i008p00653, 1978.
- 480 Bemgård, A., Colmsjö, A. and Melin, J.: Assessing breakthrough times for denuder samplers with emphasis on volatile
481 organic compounds, *J. Chromatogr. A*, 723(2), 301–311, doi:10.1016/0021-9673(95)00878-0, 1996.
- 482 Bertram, T. H., Kimmel, J. R., Crisp, T. A., Ryder, O. S., Yatavelli, R. L. N., Thornton, J. A., Cubison, M. J., Gonin, M. and
483 Worsnop, D. R.: A field-deployable, chemical ionization time-of-flight mass spectrometer, *Atmos. Meas. Tech.*, 4(7), 1471–
484 1479, doi:10.5194/amt-4-1471-2011, 2011.
- 485 Bianchi, F., Tröstl, J., Junninen, H., Frege, C., Henne, S., Hoyle, C. R., Molteni, U., Herrmann, E., Adamov, A.,
486 Bukowiecki, N., Chen, X., Duplissy, J., Gysel, M., Hutterli, M., Kangasluoma, J., Kontkanen, J., Kurten, A., Manninen, H.



- 487 E., Munch, S., Perakyla, O., Petaja, T., Rondo, L., Williamson, C., Weingartner, E., Curtius, J., Worsnop, D. R., Kulmala,
488 M., Dommen, J. and Baltensperger, U.: New particle formation in the free troposphere: A question of chemistry and timing,
489 *Science* (80-.), 352(6289), 1109–1112, doi:10.1126/science.aad5456, 2016.
- 490 Breitenlechner, M., Fischer, L., Hainer, M., Heinritzi, M., Curtius, J. and Hansel, A.: PTR3: An Instrument for Studying the
491 Lifecycle of Reactive Organic Carbon in the Atmosphere, *Anal. Chem.*, 89(11), 5824–5831,
492 doi:10.1021/acs.analchem.6b05110, 2017.
- 493 Brophy, P. and Farmer, D. K.: Clustering, methodology, and mechanistic insights into acetate chemical ionization using
494 high-resolution time-of-flight mass spectrometry, *Atmos. Meas. Tech.*, 9(8), 3969–3986, doi:10.5194/amt-9-3969-2016,
495 2016.
- 496 Curtius, J.: Nucleation of atmospheric aerosol particles, *Comptes Rendus Phys.*, 7(9–10), 1027–1045,
497 doi:10.1016/j.crhy.2006.10.018, 2006.
- 498 Duplissy, J., Merikanto, J., Franchin, A., Tsagkogeorgas, G., Kangasluoma, J., Wimmer, D., Vuollekoski, H.,
499 Schobesberger, S., Lehtipalo, K., Flagan, R. C., Brus, D., Donahue, N. M., Vehkamäki, H., Almeida, J., Amorim, A.,
500 Barmet, P., Bianchi, F., Breitenlechner, M., Dunne, E. M., Guida, R., Henschel, H., Junninen, H., Kirkby, J., Kürten, A.,
501 Kupc, A., Määttä, A., Makhmutov, V., Mathot, S., Nieminen, T., Onnela, A., Praplan, A. P., Riccobono, F., Rondo, L.,
502 Steiner, G., Tome, A., Walther, H., Baltensperger, U., Carslaw, K. S., Dommen, J., Hansel, A., Petäjä, T., Sipilä, M.,
503 Stratmann, F., Vrtala, A., Wagner, P. E., Worsnop, D. R., Curtius, J. and Kulmala, M.: Effect of ions on sulfuric acid-water
504 binary particle formation: 2. Experimental data and comparison with QC-normalized classical nucleation theory, *J. Geophys.*
505 *Res. Atmos.*, (121), 1752–1775, doi:10.1002/2015JD023538.Effect, 2016.
- 506 Ehn, M., Junninen, H., Petäjä, T., Kurtén, T., Kerminen, V. M., Schobesberger, S., Manninen, H. E., Ortega, I. K.,
507 Vehkamäki, H., Kulmala, M. and Worsnop, D. R.: Composition and temporal behavior of ambient ions in the boreal forest,
508 *Atmos. Chem. Phys.*, 10(17), 8513–8530, doi:10.5194/acp-10-8513-2010, 2010.
- 509 Ehrhart, S., Ickes, L., Almeida, J., Amorim, A., Barmet, P., Bianchi, F., Dommen, J., Dunne, E. M., Duplissy, J., Franchin,
510 A., Kangasluoma, J., Kirkby, J., Kürten, A., Kupc, A., Lehtipalo, K., Nieminen, T., Riccobono, F., Rondo, L.,
511 Schobesberger, S., Steiner, G., Tomé, A., Wimmer, D., Baltensperger, U., Wagner, P. E. and Curtius, J.: Comparison of the
512 SAWNUC model with CLOUD measurements of sulphuric acid-water nucleation, *J. Geophys. Res.*, 121(20), 12,401–12,414,
513 doi:10.1002/2015JD023723, 2016.
- 514 Eisele, F.: First tandem mass spectrometric measurement of tropospheric ions, *J. Geophys. Res. Atmos.*, 93, 716–724,
515 doi:10.1029/JD093iD01p00716, 1988.
- 516 Eisele, F. and Tanner, D.: Identification of ions in continental air, *J. Geophys. Res. Atmos.*, 95, 539, doi:Doi
517 10.1029/Jd095id12p20539, 1990.
- 518 Eisele, F. L.: Identification of tropospheric ions, *J. Geophys. Res. Atmos.*, 91(D7), 7897–7906,
519 doi:10.1029/jd091id07p07897, 1986.
- 520 Ferguson, E. E. and Arnold, F.: Ion Chemistry of the Stratosphere, *Acc. Chem. Res.*, 14(11), 327–334,



- 521 doi:10.1021/ar00071a001, 1981.
- 522 Flagan, R. C.: History of Electrical Aerosol Measurements, *Aerosol Sci. Technol.*, 28(4), 301–380,
- 523 doi:10.1080/02786829808965530, 1998.
- 524 Gerlich, D.: Inhomogeneous RF Fields: A Versatile Tool for the Study of Processes with Slow Ions, in *Advances in*
- 525 *Chemical Physics*, Volume 82, vol. LXXXII, pp. 1–176., 1992.
- 526 Gerlich, D.: Applications of rf fields and collision dynamics in atomic mass spectrometry, *J. Anal. At. Spectrom.*, 19(5),
- 527 581–590, doi:10.1039/b404032p, 2004.
- 528 Heinritzi, M., Simon, M., Steiner, G., Wagner, A. C., Kürten, A., Hansel, A. and Curtius, J.: Characterization of the mass-
- 529 dependent transmission efficiency of a CIMS, *Atmos. Meas. Tech.*, 9(4), 1449–1460, doi:10.5194/amt-9-1449-2016, 2016.
- 530 Hirsikko, A., Nieminen, T., Gagné, S., Lehtipalo, K., Manninen, H. E., Ehn, M., Hörrak, U., Kerminen, V. M., Laakso, L.,
- 531 McMurry, P. H., Mirme, A., Mirme, S., Petäjä, T., Tammet, H., Vakkari, V., Vana, M. and Kulmala, M.: Atmospheric ions
- 532 and nucleation: A review of observations, *Atmos. Chem. Phys.*, 11(2), 767–798, doi:10.5194/acp-11-767-2011, 2011.
- 533 Iyer, S., Lopez-Hilfiker, F., Lee, B. H., Thornton, J. A. and Kurtén, T.: Modeling the Detection of Organic and Inorganic
- 534 Compounds Using Iodide-Based Chemical Ionization, *J. Phys. Chem. A*, 120(4), 576–587, doi:10.1021/acs.jpca.5b09837,
- 535 2016.
- 536 Junninen, H., Ehn, M., Petäjä, Luosujärvi, L., Kotiaho, T., Kostianen, R., Rohner, U., Gonin, M., Fuhrer, K., Kulmala, M.
- 537 and Worsnop, D. R.: A high-resolution mass spectrometer to measure atmospheric ion composition, *Atmos. Meas. Tech.*,
- 538 3(4), 1039–1053, doi:10.5194/amt-3-1039-2010, 2010.
- 539 Kirkby, J., Curtius, J., Almeida, J., Dunne, E., Duplissy, J., Ehrhart, S., Franchin, A., Gagné, S., Ickes, L., Kürten, A., Kupc,
- 540 A., Metzger, A., Riccobono, F., Rondo, L., Schobesberger, S., Tsagkogeorgas, G., Wimmer, D., Amorim, A., Bianchi, F.,
- 541 Breitenlechner, M., David, A., Dommen, J., Downard, A., Ehn, M., Flagan, R. C., Haider, S., Hansel, A., Hauser, D., Jud,
- 542 W., Junninen, H., Kreissl, F., Kvashin, A., Laaksonen, A., Lehtipalo, K., Lima, J., Lovejoy, E. R., Makhmutov, V., Mathot,
- 543 S., Mikkilä, J., Minginette, P., Mogo, S., Nieminen, T., Onnela, A., Pereira, P., Petäjä, T., Schnitzhofer, R., Seinfeld, J. H.,
- 544 Sipilä, M., Stozhkov, Y., Stratmann, F., Tomé, A., Vanhanen, J., Viisanen, Y., Virtala, A., Wagner, P. E., Walther, H.,
- 545 Weingartner, E., Wex, H., Winkler, P. M., Carslaw, K. S., Worsnop, D. R., Baltensperger, U. and Kulmala, M.: Role of
- 546 sulphuric acid, ammonia and galactic cosmic rays in atmospheric aerosol nucleation, *Nature*, 476(7361), 429–435,
- 547 doi:10.1038/nature10343, 2011.
- 548 Kirkby, J., Duplissy, J., Sengupta, K., Frege, C., Gordon, H., Williamson, C., Heinritzi, M., Simon, M., Yan, C., Almeida, J.,
- 549 Trostl, J., Nieminen, T., Ortega, I. K., Wagner, R., Adamov, A., Amorim, A., Bernhammer, A. K., Bianchi, F.,
- 550 Breitenlechner, M., Brilke, S., Chen, X., Craven, J., Dias, A., Ehrhart, S., Flagan, R. C., Franchin, A., Fuchs, C., Guida, R.,
- 551 Hakala, J., Hoyle, C. R., Jokinen, T., Junninen, H., Kangasluoma, J., Kim, J., Krapf, M., Kurten, A., Laaksonen, A.,
- 552 Lehtipalo, K., Makhmutov, V., Mathot, S., Molteni, U., Onnela, A., Perakyla, O., Piel, F., Petaja, T., Praplan, A. P., Pringle,
- 553 K., Rap, A., Richards, N. A. D., Riipinen, I., Rissanen, M. P., Rondo, L., Sarnela, N., Schobesberger, S., Scott, C. E.,
- 554 Seinfeld, J. H., Sipilä, M., Steiner, G., Stozhkov, Y., Stratmann, F., Tomé, A., Virtanen, A., Vogel, A. L., Wagner, A. C.,



- 555 Wagner, P. E., Weingartner, E., Wimmer, D., Winkler, P. M., Ye, P., Zhang, X., Hansel, A., Dommen, J., Donahue, N. M.,
556 Worsnop, D. R., Baltensperger, U., Kulmala, M., Carslaw, K. S. and Curtius, J.: Ion-induced nucleation of pure biogenic
557 particles, *Nature*, 533(7604), 521–526, doi:10.1038/nature17953, 2016.
- 558 Kürten, A., Jokinen, T., Simon, M., Sipilä, M., Sarnela, N., Junninen, H., Adamov, A., Almeida, J., Amorim, A., Bianchi, F.,
559 Breitenlechner, M., Dommen, J., Donahue, N. M., Duplissy, J., Ehrhart, S., Flagan, R. C., Franchin, A., Hakala, J., Hansel,
560 A., Heinritzi, M., Hutterli, M., Kangasluoma, J., Kirkby, J., Laaksonen, A., Lehtipalo, K., Leiminger, M., Makhmutov, V.,
561 Mathot, S., Onnela, A., Petäjä, T., Praplan, A. P., Riccobono, F., Rissanen, M. P., Rondo, L., Schobesberger, S., Seinfeld, J.
562 H., Steiner, G., Tomé, A., Tröstl, J., Winkler, P. M., Williamson, C., Wimmer, D., Ye, P., Baltensperger, U., Carslaw, K. S.,
563 Kulmala, M., Worsnop, D. R. and Curtius, J.: Neutral molecular cluster formation of sulfuric acid–dimethylamine observed
564 in real time under atmospheric conditions, *Proc. Natl. Acad. Sci.*, 111(42), 15019–15024, doi:10.1073/pnas.1404853111,
565 2014.
- 566 Lopez-Hilfiker, F. D., Iyer, S., Mohr, C., Lee, B. H., D’ambro, E. L., Kurtén, T. and Thornton, J. A.: Constraining the
567 sensitivity of iodide adduct chemical ionization mass spectrometry to multifunctional organic molecules using the collision
568 limit and thermodynamic stability of iodide ion adducts, *Atmos. Meas. Tech.*, 9(4), 1505–1512, doi:10.5194/amt-9-1505-
569 2016, 2016.
- 570 Meot-Ner, M. and Sieck, L. W.: The Ionic Hydrogen Bond and Ion Solvation. 5. OH···O- Bonds. Gas-Phase Solvation and
571 Clustering of Alkoxide and Carboxylate Anions, *J. Am. Chem. Soc.*, 108(24), 7525–7529, doi:10.1021/ja00284a014, 1986.
- 572 Meot-Ner, M. M.: The Ionic Hydrogen Bond and Ion Solvation. 2. Solvation of Onium Ions by One to Seven H₂O
573 Molecules. Relations between Monomolecular, Specific, and Bulk Hydration, *J. Am. Chem. Soc.*, 106(5), 1265–1272,
574 doi:10.1021/ja00317a016, 1984.
- 575 Müller, M., Mikoviny, T., Feil, S., Haidacher, S., Hanel, G., Hartungen, E., Jordan, A., Märk, L., Mutschlechner, P.,
576 Schottkowsky, R., Sulzer, P., Crawford, J. H. and Wisthaler, A.: A compact PTR-ToF-MS instrument for airborne
577 measurements of volatile organic compounds at high spatiotemporal resolution, *Atmos. Meas. Tech.*, 7(11), 3763–3772,
578 doi:10.5194/amt-7-3763-2014, 2014.
- 579 Olenius, T., Schobesberger, S., Kupiainen-Määttä, O., Franchin, A., Junninen, H., Ortega, I. K., Kurtén, T., Loukonen, V.,
580 Worsnop, D. R., Kulmala, M. and Vehkamäki, H.: Comparing simulated and experimental molecular cluster distributions,
581 *Faraday Discuss.*, 165, 75, doi:10.1039/c3fd00031a, 2013.
- 582 Perkins, M. D. and Eisele, F. L.: First Mass Spectrometric Measurements of Atmospheric Ions At Ground Level., *J.*
583 *Geophys. Res.*, 89(D6), 9649–9657, doi:10.1029/JD089iD06p09649, 1984.
- 584 Rus, J., Moro, D., Sillero, J. A., Royuela, J., Casado, A., Estevez-Molinero, F. and Fernández de la Mora, J.: IMS-MS
585 studies based on coupling a differential mobility analyzer (DMA) to commercial API-MS systems, *Int. J. Mass Spectrom.*,
586 298(1–3), 30–40, doi:10.1016/j.ijms.2010.05.008, 2010.
- 587 Schnitzhofer, R., Metzger, A., Breitenlechner, M., Jud, W., Heinritzi, M., De Menezes, L. P., Duplissy, J., Guida, R., Haider,
588 S., Kirkby, J., Mathot, S., Minginette, P., Onnela, A., Walther, H., Wasem, A. and Hansel, A.: Characterisation of organic



589 contaminants in the CLOUD chamber at CERN, *Atmos. Meas. Tech.*, 7(7), 2159–2168, doi:10.5194/amt-7-2159-2014,
590 2014.

591 Schobesberger, S., Junninen, H., Bianchi, F., Lonn, G., Ehn, M., Lehtipalo, K., Dommen, J., Ehrhart, S., Ortega, I. K.,
592 Franchin, A., Nieminen, T., Riccobono, F., Hutterli, M., Duplissy, J., Almeida, J., Amorim, A., Breitenlechner, M.,
593 Downard, A. J., Dunne, E. M., Flagan, R. C., Kajos, M., Keskinen, H., Kirkby, J., Kupc, A., Kurten, A., Kurten, T.,
594 Laaksonen, A., Mathot, S., Onnela, A., Praplan, A. P., Rondo, L., Santos, F. D., Schallhart, S., Schnitzhofer, R., Sipila, M.,
595 Tome, A., Tsagkogeorgas, G., Vehkamäki, H., Wimmer, D., Baltensperger, U., Carslaw, K. S., Curtius, J., Hansel, A.,
596 Petaja, T., Kulmala, M., Donahue, N. M. and Worsnop, D. R.: Molecular understanding of atmospheric particle formation
597 from sulfuric acid and large oxidized organic molecules, *Proc. Natl. Acad. Sci.*, 110(43), 17223–17228,
598 doi:10.1073/pnas.1306973110, 2013.

599 Sipilä, M., Sarnela, N., Jokinen, T., Henschel, H., Junninen, H., Kontkanen, J., Richters, S., Kangasluoma, J., Franchin, A.,
600 Peräkylä, O., Rissanen, M. P., Ehn, M., Vehkamäki, H., Kurten, T., Berndt, T., Petäjä, T., Worsnop, D., Ceburnis, D.,
601 Kerminen, V. M., Kulmala, M. and O’Dowd, C.: Molecular-scale evidence of aerosol particle formation via sequential
602 addition of HIO₃, *Nature*, 537(7621), 532–534, doi:10.1038/nature19314, 2016.

603 Steiner, G., Attoui, M., Wimmer, D. and Reischl, G. P.: A medium flow, high-resolution Vienna DMA running in
604 recirculating mode, *Aerosol Sci. Technol.*, 44(4), 308–315, doi:10.1080/02786821003636763, 2010.

605 Ude, S. and De La Mora, J. F.: Molecular monodisperse mobility and mass standards from electrosprays of tetra-alkyl
606 ammonium halides, *J. Aerosol Sci.*, 36(10), 1224–1237, doi:10.1016/j.jaerosci.2005.02.009, 2005.

607 Viggiano, A. A. and Arnold, F.: The first height measurements of the negative ion composition of the stratosphere, *Planet.*
608 *Space Sci.*, 29(8), 895–906, doi:10.1016/0032-0633(81)90079-9, 1981.

609 Winklmayr, W., Reischl, G. P., Lindner, A. O. and Berner, A.: A new electromobility spectrometer for the measurement of
610 aerosol size distributions in the size range from 1 to 1000 nm, *J. Aerosol Sci.*, 22(3), 289–296, doi:10.1016/S0021-
611 8502(05)80007-2, 1991.

612 Zapadinsky, E., Passananti, M., Myllys, N., Kurtén, T. and Vehkamäki, H.: Modeling on Fragmentation of Clusters inside a
613 Mass Spectrometer, *J. Phys. Chem. A*, doi:10.1021/acs.jpca.8b10744, 2019.

614

615

616



Ion guide properties	Quadrupole (2n=4)	Hexapole (2n=6)	Octopole (2n=8)	Higher order multipoles (2n>8)
Focusing power	High	Medium	Low	Lower
Field free region	Low	Medium	High	Higher
Mass range	Low	Medium	High	Higher

617 **Table 1:** Qualitative comparison of the ion guide transfer properties of ideal multipoles with 2n poles (Gerlich, 1992).

618

619

Name	Sum formula	Monomer A ⁺ (AB) ₀ m/z [Th] (d _z [nm])	Dimer A ⁺ (AB) ₁ m/z [Th] (d _z [nm])	Trimer A ⁺ (AB) ₂ m/z [Th] (d _z [nm])	Tetramer A ⁺ (AB) ₃ m/z [Th] (d _z [nm])
TMAI	C ₄ H ₁₂ NI	74.097 (1.05)			
TPrAI	C ₁₂ H ₂₈ NI	186.222 (1.16)	499.349 (1.45)	812.475 (1.66)	
TBAI	C ₁₆ H ₃₆ NI	242.285 (1.24)	611.474 (1.55)	980.663 (1.73)	
THABr	C ₂₈ H ₆₀ NBr	410.473 (1.47)	899.863 (1.78)	1389.254 (1.97)	
IL	C ₁₅ H ₃₀ F ₆ N ₂ O ₄ S ₂	200.238 (1.15*)	680.393 (1.5*)	1160.703 (1.7*)	1640.703 (1.9*)

620 **Table 2.** Positive cluster ions, their corresponding mass-to-charge ratio m/z and the mobility diameter d_z of Tetra-Methyl-Ammonium-Iodine
 621 (TMAI), Tetra-Propyl-Ammonium-Iodine (TPrAI), Tetra-Butyl-Ammonium-Iodine (TBAI), Tetra-Heptyl-Ammonium-Bromide (THABr)
 622 and Tributylmethylammonium-bis(trifluoromethylsulfonyl)imide (ionic liquid: IL) used in this work. A is the tetra-alkyl-ammonium part of
 623 the neutral molecule, while B can be I or Br in the case of the first four compounds. *The mobility diameters for the ionic liquid were
 624 determined in this study with an uncertainty of ±0.1 nm.

625

	ioniAPi-TOF UIBK	UEF APi-TOF
Type of multipoles	Hexapole	Quadrupole
Multipole configuration	Straight and geometrically identical hexapoles	A short (SSQ) and a big (BSQ) segmented quadrupole
Diameter of critical orifice at MS entrance [mm]	0.4	0.3
Flow rate through orifice [L/min]	1.1	0.8
TOF-platform	ioniTOF1000, IONICON Analytik GmbH	H-TOF, Tofwerk AG
Mass resolution (FWHM)	1500-2000	~5000
Extraction frequency [kHz]	30	12.5

626 **Table 3:** Main technical differences of the ioniAPi-TOF UIBK compared to the UEF APi-TOF relevant for this study (Junninen et al.,
 627 2010). Mass resolution and extraction frequency are setting dependent. Shown values were used during the CLOUD 12 campaign and
 628 therefore valid for the inter-comparison in section 3.3.



629

	ΔG (T=298K)	$-\Delta H$	dV_{50}
	[kcal/mol]	[kcal/mol]	[V]
$H_3O^+(H_2O)_1$	-24.2	31.5	
$H_3O^+(H_2O)_2$	-13.4	20	-7.5
$H_3O^+(H_2O)_3$	-9	17	-5.6

630 **Table 4:** Gibbs free energies, binding energies ($BE(H_3O^+(H_2O)_{1-3}) = -\Delta H$) and corresponding dV_{50} for $H_3O^+(H_2O)_{1-3}$ clusters (Meot-
 631 Ner, 1984).

632

633

run number	temperature	rel. humidity	ions	NH_3	SO_2	O_3	$C_{10}H_{16}$	C_5H_8
	[K]	[%]	[cm^{-3}]	[ppbv]	[ppbv]	[ppbv]	[ppbv]	[ppbv]
1963.15	223	99	~2000	0	0	38	0.2	2.8

634

Table 5: Experimental conditions for the inter-comparison during run 1963.15 at the CLOUD experiment, CERN.

635

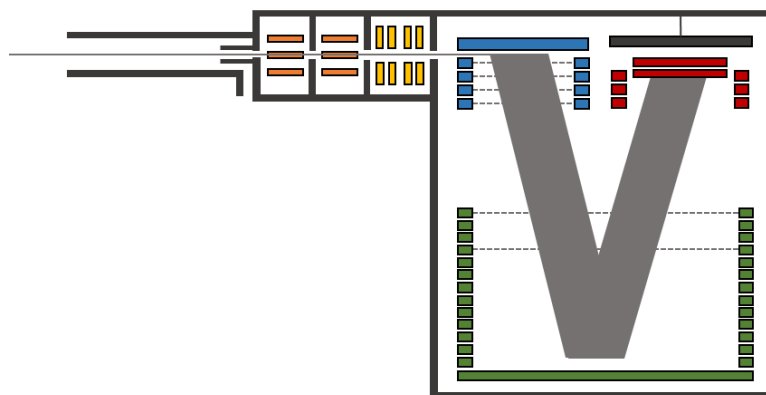


636

637

638

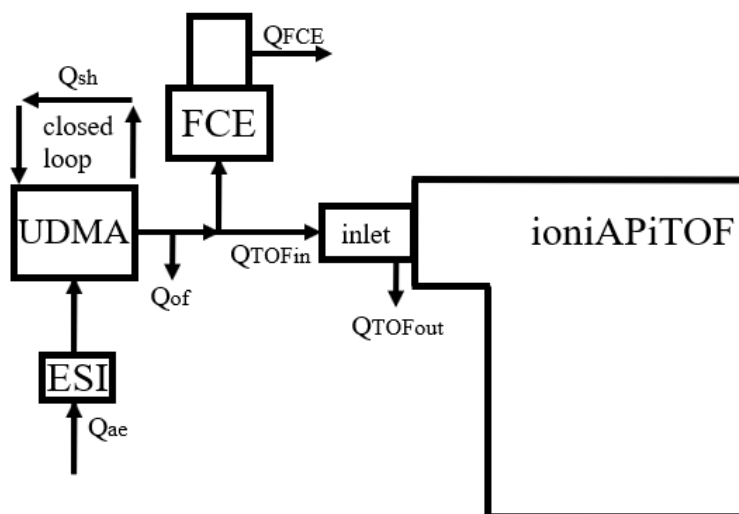
639



640

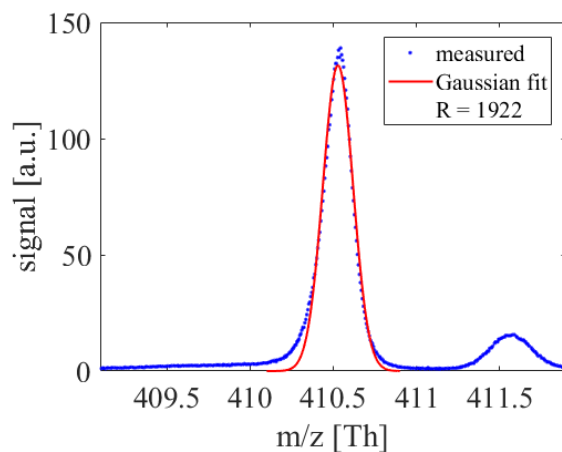
641 **Figure 1:** Schematic of the ioniAPi-TOF mass spectrometer. The hexapoles are shown in orange and the ion optical lens system in yellow.
642 The orthogonal extraction region is coloured in blue. The reflectron is coloured in green and the detection region with post acceleration
643 and MCP in red.

644



645

646 **Figure 2:** Experimental setup of the Cluster-Calibration Unit consisting of an electrospray ionisation source (ESI), a differential mobility
647 analyser (UDMA) and a Faraday cup electrometer (FCE) (Steiner et al., 2010; Winklmayr et al., 1991). Although not shown here, the flow
648 to both detectors is split via a Y-splitter with an angle of 20° for both sampling lines downstream to reduce inhomogeneity's that might
649 occur due to the flow separation.



650

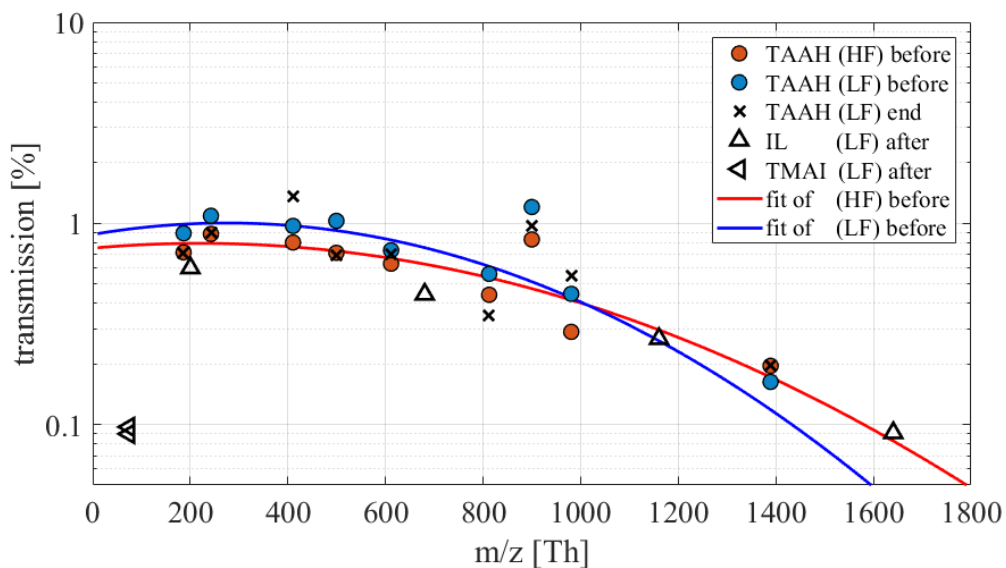
651

652

Figure 3: The mass resolution of the ioniAPi-TOF is about 2000 at a nominal mass of 410 Th, which corresponds to $C_{28}H_{60}N^+$, the THABr monomer.

653

654



655

656

657

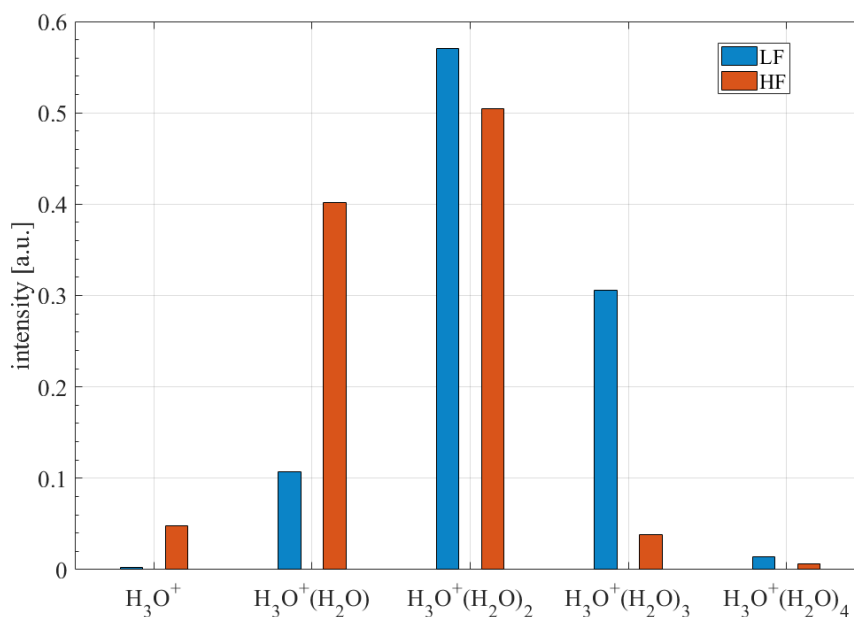
658

Figure 4: Transmission efficiency for low (LF) and high (HF) fragmenting ion transfer settings of the ioniAPi-TOF for ions of different Tetra-Alkyl-Ammonium-Halides (TAAH) and an ionic liquid (IL), see Table 2. A Gaussian fit was used to obtain the transmission curves. Calibrations were done before the CLOUD campaign, in the end and after the campaign in Innsbruck.

659



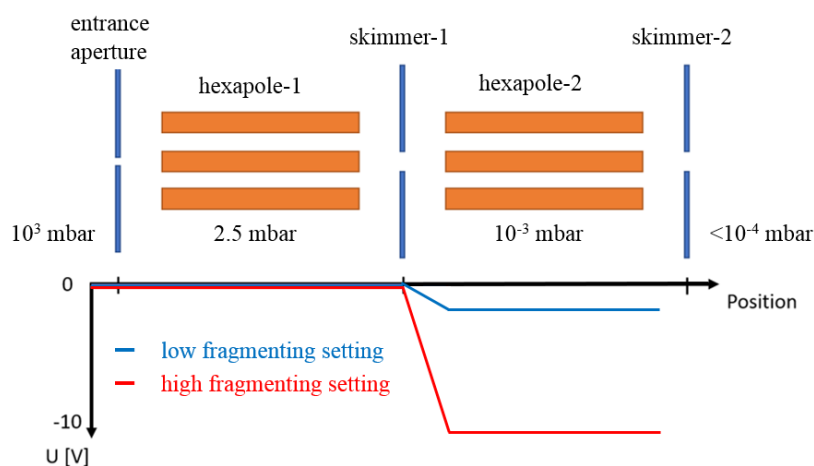
660



661

662 **Figure 5:** Comparison of the low fragmenting (LF, voltage difference: $dV = -1.4$ V) and the high fragmenting (HF, voltage difference:
 663 $dV = -10.0$ V) setting. Ion counts are corrected for transmission effects and normalised for each setting.

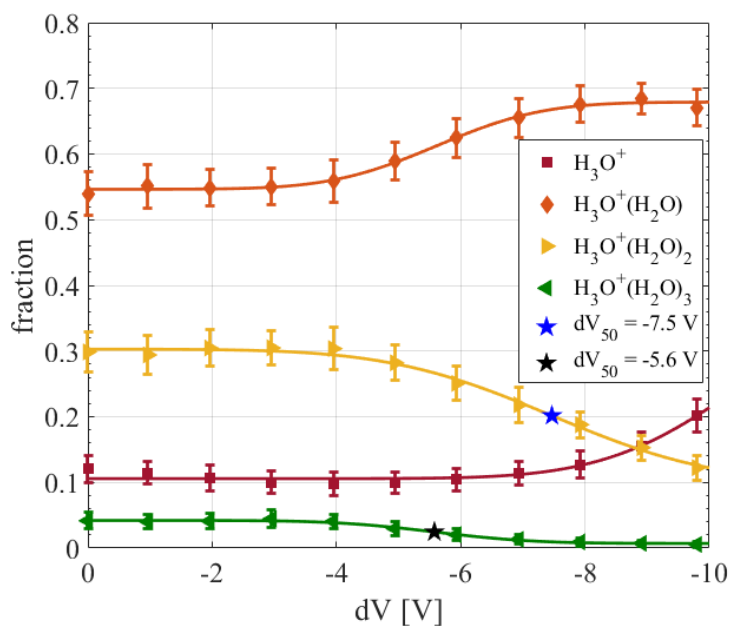
664



665

666 **Figure 6:** Schematic of the region inside the ionAPI-TOF mass spectrometer where fragmentation was studied in this work. Here, a low
 667 fragmenting clustered setting and a high fragmenting declustering setting can be used to identify cluster ions and to study their stability by
 668 adjusting the voltage difference dV between skimmer-1 and hexapole-2.

669



670

671

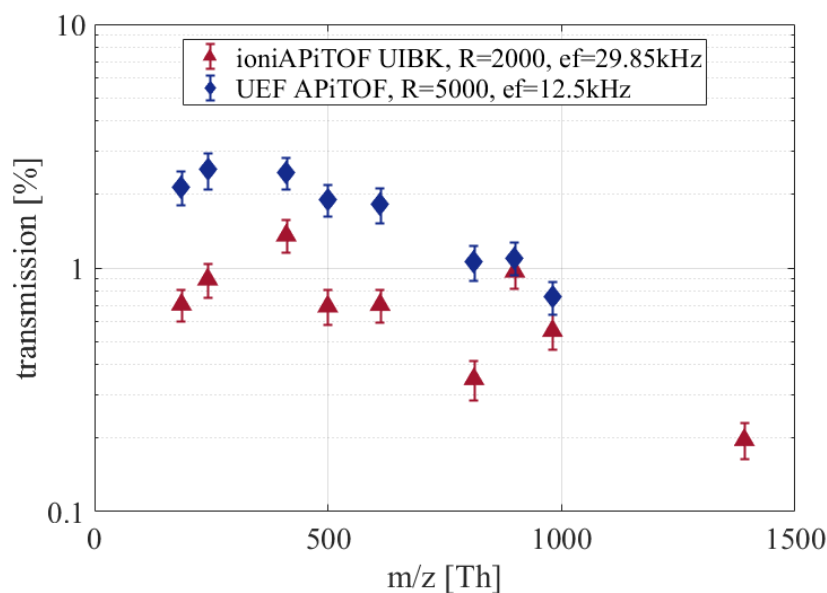
672

673

Figure 7: Declustering (dV) scan between the skimmer-1 and the second hexapole using hydrated hydronium clusters. Peak intensities are normalised. The dV_{50} of $H_3O^+(H_2O)_3$ is -5.6 V and the one of $H_3O^+(H_2O)_2$ is -7.5 V. The low fragmenting setting uses a dV of -1.4 V, whereas -10 V are used for the high fragmenting setting.

674

675

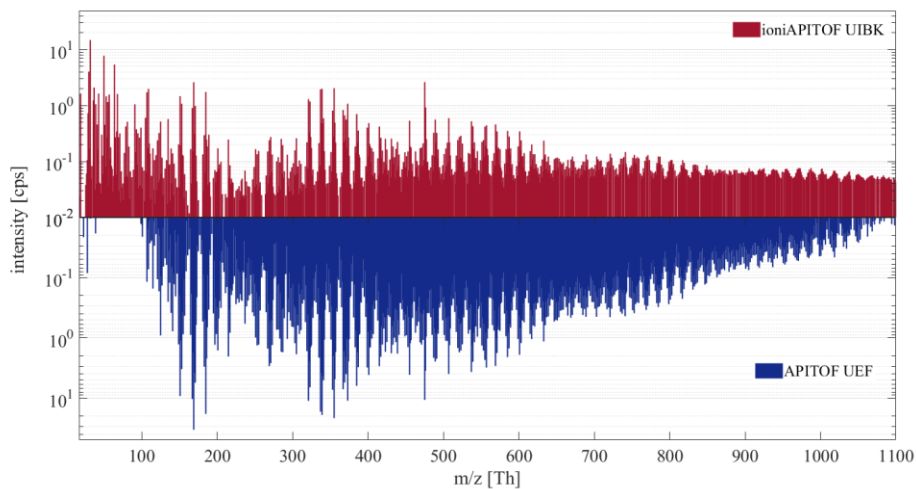


676

677

678

Figure 8: Comparison of the ioniAPi-TOF and the UEF APi-TOF regarding the transmission efficiency. The UEF APi-TOF is set to high-mass range settings (m/z 100-2000 Th). The extraction frequencies ef varies with the length of the TOF mass analyser.



679

680

681

682

Figure 9: Comparison of the mass spectra obtained during run 1963.15 at the CLOUD experiment at CERN of the ioniAPi-TOF and the UEF APi-TOF.